Excitation of Weakly Bound Molecules to Trilobitelike Rydberg States

M. A. Bellos,* R. Carollo, J. Banerjee, E. E. Eyler, P. L. Gould, and W. C. Stwalley
Department of Physics, University of Connecticut, Storrs, Connecticut 06269-3046, USA
(Received 12 March 2013; published 29 July 2013)

We observe "trilobitelike" states of ultracold $^{85}Rb_2$ molecules, in which a ground-state atom is bound by the electronic wave function of its Rydberg-atom partner. We populate these states through the ultraviolet excitation of weakly bound molecules, and access a regime of trilobitelike states at low principal quantum numbers and with vibrational turning points around 35 Bohr radii. This demonstrates that, unlike previous studies that used free-to-bound transitions, trilobitelike states can also be excited through bound-to-bound transitions. This approach provides high excitation probabilities without requiring high-density samples, and affords the ability to control the excitation radius by selection of the initial-state vibrational level.

DOI: 10.1103/PhysRevLett.111.053001 PACS numbers: 33.80.Rv, 31.10.+z, 33.20.Lg, 67.85.−d

A class of long-range Rydberg molecules, sometimes called "trilobite molecules," occurs when a ground-state atom is embedded within the electronic wave function of a Rydberg atom [1]. The bond between the Rydberg atom and the ground-state atom originates from the attractive interaction between the Rydberg electron and the ground-state atom [1]. This bond has been described as a new type of chemical bond, distinct from the well-known covalent, ionic, and van der Waals bonds [2]. The name "trilobite molecule" was coined because in certain states, the perturbed Rydberg-electron wave function resembles a trilobite fossil [1]. Trilobite states are characterized by large, and degenerate, values of orbital angular momentum ($l \geq 3$) and large permanent electric dipole moments (EDMs $\sim$1 kD). Although pure trilobite states have yet to be observed, *trilobitelike* states, bound by the same novel chemical bond but characterized primarily by lower values of l and smaller EDMs, have been observed at ultracold temperature in photoassociation to bound vibrational levels [3–8], and at high temperatures in the form of satellite structures in the wings of atomic transitions [9,10].

We adopt the name "trilobitelike" molecules for the low-l states to distinguish them from other types of long-range Rydberg molecules, such as macrodimers [11–13] or heavy Rydberg atoms [14,15].

The bond length of a trilobitelike molecule can vary greatly depending on the principal quantum number due to the n^2 dependence of the radius of the outermost lobe of the Rydberg wave function. For instance, the vibrational outer turning points of trilobitelike molecules have ranged from below 150 Bohr radii (a_0) in Refs. [9,10] to above $10^3 a_0$ in Refs. [3–8].

Here we report the observation of trilobitelike states of $^{85}Rb_2$ by a new method. We start by producing ultracold Rb_2 molecules in a high vibrational level of the metastable $a\,^3\Sigma_u^+$ state via photoassociation of atoms in a magneto-optical trap (MOT), then excite them directly to trilobitelike states, detecting them via their autoionization into Rb_2^+ molecular ions. We observe these states in some of the lowest principal quantum numbers for which they can exist, $n = 7$ and 9–12, and also for some of the shortest internuclear separations at which they can form. As far as we are aware, this is the first time that trilobitelike states have been produced via bound-bound molecular transitions.

The range we have investigated overlaps with previous studies conducted in heat-pipe ovens [9,10], in which satellite structures in the line wings of collisionally broadened Rb were found to correspond closely with minima of calculated long-range potential energy curves (PECs) [9]. Although we access some of the same PECs, there are notable differences in the excitation pathway, detection scheme, and the attainable linewidth.

The low-l trilobitelike binding energy (in atomic units) between the Rydberg electron and the embedded atom can be approximated by

$$V(R) = 2\pi a_s |\psi(R)|^2 + 6\pi a_p^3 |\nabla\psi(R)|^2, \qquad (1)$$

where $\psi(R)$ is the unperturbed Rydberg-electron wave function, and a_s and a_p are the energy-dependent (and therefore R-dependent) s- and p-wave scattering lengths, respectively, for low-energy collisions between the electron and the embedded atom [4,16,17]. The first term of Eq. (1) originates from s-wave scattering, and the second from p-wave scattering. In the low-n small-R regime of Rb_2, the second term is dominant as the p-wave scattering length is strongly influenced by the presence of an electron +atom shape resonance [17–19]. However, for interactions in the high-n large-R regime the first term can dominate, such as when the kinetic energy of the Rydberg electron is too small to support p-wave collisions [20].

For a Rydberg electron in quantum state $|l = 1, m = 0\rangle$, the $|\nabla\psi(R)|^2$ term in Eq. (1) is proportional to $[\partial\psi(R)/\partial R]^2$ and correlates to PECs of $^3\Sigma^+$ symmetry as shown in Fig. 1. In the case of an electron in quantum state $|l = 1, m = \pm 1\rangle$, the $|\nabla\psi(R)|^2$ term is instead

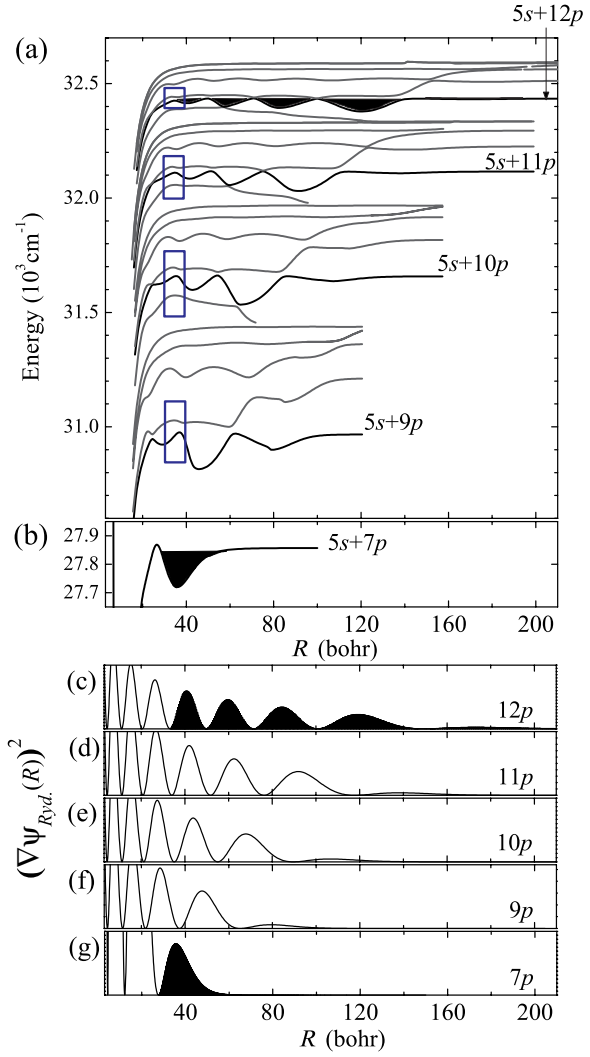

FIG. 1 (color online). (a) $^3\Sigma^+$ excited-state potential energy curves from Ref. [9] calculated through Fermi pseudopotential methods. The rectangular boxes label the outer turning points of states populated in the present work, which are replotted in greater detail in Fig. 3. (b) $^3\Sigma_g^+$ excited-state potential energy curve from Ref. [24] calculated through *ab initio* methods. (c)–(g) Derivatives of the radial Rydberg-electron wave functions for $12p$, $11p$, $10p$, $9p$, and $7p$ atoms, respectively. The Rydberg-electron wave functions are approximated by phase-shifted hydrogenic wave functions calculated using Numerov integration in square-root coordinates [31]. The shaded regions illustrate the correlation between potential wells and oscillations of the electron wave function derivatives.

proportional to $[\psi(R)/R]^2$ and correlates to PECs of $^3\Pi$ symmetry. Such correlations between PECs and the Rydberg-electron wave functions also occur in the undulations of *ab initio* excited-state PECs, showing that conventional *ab initio* PECs can reproduce the low-n trilobitelike bond [21]. In principle, the excited-state PECs of all molecules could exhibit these undulations, as long as the scattering length between the Rydberg electron and embedded atom is nonzero. In Rb_2, and other alkali-metal dimers such as Cs_2 and Fr_2, the existence of a p-wave triplet shape resonance [18,19] produces large p-wave scattering lengths. As a result, Rb_2 has low-n potential wells that can exceed 100 cm^{-1} in depth [9], and support over 100 vibrational levels. Unlike the case of high-n large-R trilobitelike states, a large number of vibrational levels is supported in each well and tunneling between wells is not significant due to the large barriers between wells.

In Fig. 1(a) we plot the relevant excited-state PECs from Ref. [9], which were calculated using the Fermi pseudopotential method. These trilobitelike states, due to their EDMs, do not have *ungerade-gerade* symmetry [1,7]. The curves do not extend into the short-range region, because the Fermi pseudopotential model breaks down at separations where covalent bonding appears. Despite this breakdown, these Fermi pseudopotential curves are consistent with our observations, which are dominated by excitation around $R = 35a_0$. We have converted the difference potentials of Ref. [9] (which characterize free-bound excitation) back to full excited-state potentials (which characterize bound-bound excitation) by simply adding the long-range ground-state potential energy [22]. In Fig. 1(b) we plot the relevant *ab initio* excited-state PEC for the $5s + 7p$ asymptote [23]. Observations of the low-n medium-R regime should allow detailed comparison of the *ab initio* and Fermi pseudopotential methods at the extremes of their applicability.

The apparatus and procedure for initial state preparation have been previously described in Ref. [24] and are only briefly summarized here. The starting point is a MOT that traps about 8×10^7 ^{85}Rb atoms at a peak density of 1×10^{11} cm^{-3} and a temperature of 120 μK. We form excited-state molecules by photoassociating atom pairs into the level $|1(0_g^-), v' \simeq 173, J' = 1\rangle$ using a cw laser tuned to 796 nm [25]. We rely on spontaneous emission to produce weakly bound $J = 0$ and $J = 2$ molecules, most of which populate the single vibrational level $|a\,^3\Sigma_u^+, v = 35\rangle$, with a binding energy of $E_B = -0.8$ cm^{-1} relative to the $5s + 5s$ ground-state atomic limit [24]. We use this weakly bound level as the starting point for excitation to trilobitelike states. Although molecules are continuously produced in the MOT by the PA laser, they are also continuously lost because they are not trapped. As the molecules free fall below the MOT, we photoexcite them with a pulsed uv laser and detect the formation of Rb_2^+ ions. A positively charged electric field plate accelerates the Rb_2^+ ions from the center of the vacuum chamber towards an ion detector, where they are distinguished from Rb^+ ions by their time of flight. The charged field plate produces an electric field at the position of the MOT of about 100 V cm^{-1}. Pulsing the electric field on immediately after the photoexcitation does not lead to observable changes in signal strength, indicating that field ionization is not the dominant ionization mechanism.

We produce the uv light by frequency doubling a pulsed dye laser, operated with a red laser dye (LDS750), to access the energy region around the $5s + 7p$ atomic limit, and with an orange laser dye (DCM) to access the higher atomic limits. We have not examined the energy region around $5s + 8p$ because the required wavelengths are more difficult to produce. Our excitation laser is well suited for broad survey scans but because its linewidth ($0.9\ \mathrm{cm}^{-1}$) is comparable to typical excited-state vibrational spacings, we are only able to resolve individual vibrational levels in favorable cases. We anticipate that order-of-magnitude gains in resolution are possible through the use of a pulse-amplified cw laser [26,27].

The production and detection of trilobitelike states can be summarized by the steps,

$$\mathrm{Rb}_2 + h\nu \rightarrow \mathrm{Rb}_2^{**} \rightarrow \mathrm{Rb}_2^{+} + e^{-}. \quad (2)$$

The first step is a single-photon bound-bound excitation, which corresponds to a change in bonding from an initial state bound primarily by van der Waals forces to a final state bound primarily by the trilobitelike bond of Eq. (1). The designation Rb_2^{**} refers to excited states of the molecule, either trilobitelike or nontrilobitelike, that are energetically above the ionization threshold and can spontaneously autoionize. We have previously deduced that our Rb_2^{+} signals arise from autoionization rather than photoionization [24]. The fact that we observe any Rb_2^{+} at all indicates that the autoionization lifetime is at least comparable to the radiative decay rate of the excited state.

The production of these trilobitelike states is quite efficient. With only a few hundred Rb_2 molecules present within the uv excitation beam, we detect up to 20 or 30 Rb_2^{+} ions per pulse, implying a probability for excitation followed by autoionization [see Eq. (2)] of roughly 10%. The high transition probability is partly due to the large vibrational wave function overlap between weakly bound molecules and the long-range trilobitelike states. Because the initial state is a single bound molecule, there is no dependence on sample density.

In Fig. 2(b) we plot the number of Rb_2^{+} ions detected per uv pulse as a function of the applied uv frequency. Broad similarities are evident between the present work and previous heat-pipe spectra [9,10], plotted in Fig. 2(a). These similarities exist despite differences in the initial conditions (hot colliding atoms vs ultracold molecules), detection mechanism (absorption vs ionization), and temperature (1000 K vs 10^{-4} K). In Figs. 3(a)–3(e) we plot the innermost wells of trilobitelike states and provide an assignment between PECs and the observed spectral features plotted in Figs. 3(g)–3(k). The broad similarities between the spectra in the present work and the structure seen previously in heat-pipe ovens [9,10] can still be observed for the lines blue of the atomic transitions to $9p$-$11p$, but not for lines red of the atomic transitions. At least some differences between our spectra and the heat-pipe observations are expected for all asymptotes above

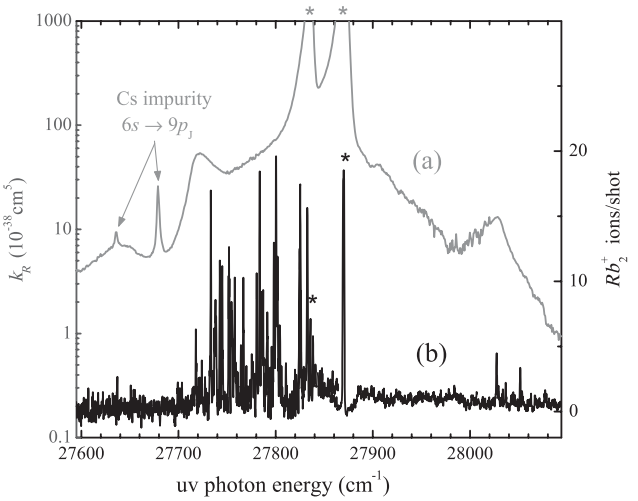

FIG. 2. (a) Reduced absorption coefficient of rubidium in a heat-pipe oven as a function of uv frequency, from Ref. [9]. The lines labeled by two arrows are atomic transitions arising from cesium contamination and are not present in our experiment. (b) Rb_2^{+} autoionization signal from laser excitation of high-v ultracold molecules (present work). Both experiments access the same excited-state region around $5s + 7p$. Lines marked with an asterisk originate from the strong atomic transitions $5s \rightarrow 7p_{1/2}$, $7p_{3/2}$. In (b), these signals are due to leakage from the Rb^{+} time-of-flight channel into the Rb_2^{+} channel, and therefore significantly underestimate the actual Rb^{+} ion production rate.

$5s + 7p$, because in the present work we excite to trilobitelike wells with internuclear separations strictly less than $R = 40a_0$. While in heat-pipe ovens, free-bound transitions can occur to any trilobitelike well at any internuclear distance. Despite the difference in the Franck-Condon overlap between bound-bound transitions and free-bound transitions, we observe that lines to the blue of the atomic transitions to $9p$-$11p$ match the energies of features observed in heat-pipe ovens. Interestingly, in Ref. [10] the feature blue of $11p$ is attributed to trilobitelike wells with $R \geq 63a_0$; however, in the present work, the line blue of the $11p$ asymptote [see Fig. 3(h)] is more logically assigned to one of the inner trilobitelike wells with $R \leq 40a_0$ [see Fig. 3(b)].

Several interesting questions remain: why have most of the observations to date been well explained by transitions to $^3\Sigma^+$ trilobitelike states, but not to $^3\Pi$ states, which are also allowed by E1 selection rules? Could some of the unassigned large features in Fig. 3 be due to these $^3\Pi$ states? In addition, by what mechanism do these trilobitelike states autoionize, given that Rb_2^{+} must be produced at short range? Trilobitelike states of Rb_2 were previously found to decay both into Rb^{+} and Rb_2^{+} ions [3–6], while those of Cs_2 were found to decay only into Cs^{+} [8]. The decay mechanism of trilobitelike states is currently not fully understood.

One of the advantages of our bound-bound excitation method is that it allows control over the Franck-Condon

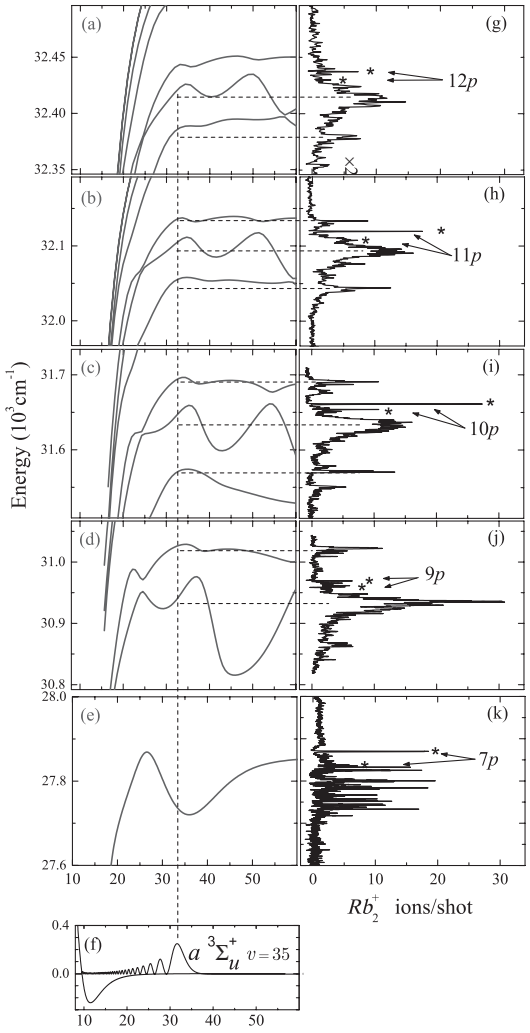

FIG. 3. (a)–(e) Close ups of the trilobitelike $^3\Sigma^+$ PECs around the $5s + np$, $n = 12$, 11, 10, 9 and 7 asymptotes, respectively, and corresponding $Rb_2{}^+$ ion spectra (g)–(k). (f) PEC and vibrational probability density of the initial $|a\,^3\Sigma_u^+, v = 35\rangle$ state. The lines marked with an asterisk denote atomic transitions from $5s$ to $np_{1/2}$, $np_{3/2}$. The dashed vertical line depicts the center of the Franck-Condon window for the transition from the last lobe of the initial-state vibrational wave function to various trilobitelike PECs. The dashed horizontal lines indicate assignments of strong spectral features to the outer turning points of selected PECs. Some of the weak lines can be traced back to the second-to-last lobe of the initial-state vibrational wave function.

overlap of the initial and final states. By choosing the initial vibrational level, an experiment can be tailored to excite predominantly a single well in a trilobitelike PEC, simplifying the spectrum and facilitating its assignment. Furthermore, by varying the outer turning point of the initial state, one can study variations of parameters across wells of the excited-state PEC, such as changes in EDM between wells, or mixing between covalent bonding at short range with trilobitelike bonding at long range.

Our present apparatus is limited in this regard because it cannot build up population in the very highest vibrational levels of the $a\,^3\Sigma_u^+$ or $X\,^1\Sigma_g^+$ state, due to inadvertent photodissociation caused by the photoassociation laser [28]. The $|a\,^3\Sigma_u^+, v = 35\rangle$ level used for this work, with its outer turning point of $35a_0$, is the highest that we can populate with reasonable numbers. This limitation could be overcome by using, for example, stimulated Raman transfer or magnetoassociation via Feshbach resonances [29] to populate the uppermost vibrational level. For instance, the last bound levels of $^{85}Rb_2$ and $^{87}Rb_2$ molecules in the $a\,^3\Sigma_u^+$ state have outer turning points of $73a_0$ and $104a_0$, respectively [30]. Magnetoassociated molecules, with their large outer turning points and rovibrational-state purity, are expected to be particularly good starting points for the population of trilobitelike states.

In conclusion, we demonstrate the production of low-n trilobitelike states through bound-to-bound excitation of weakly bound molecules. This approach is relatively simple and should be applicable to other diatomic molecules, including heteronuclear systems, and possibly to the production of trilobitelike trimers [4]. Weakly bound molecules, with their large outer turning points, can have a significant wave function overlap with long-range trilobitelike states. We find that our spectra are consistent with calculated PECs and with previously observed spectra in heat-pipe ovens. The ability to produce trilobitelike states in a low-density collision-free regime will shed light on the decay mechanism of these fragile molecules.

We thank C. H. Greene for valuable discussions, and the authors of Ref. [9] and V. Horvatic for making data available to us. We gratefully acknowledge funding from NSF and AFOSR (MURI).

*Present Address: Yale University, Department of Physics, P.O. Box 208120, New Haven, Connecticut 06520-8120, USA.

[1] C. H. Greene, A. S. Dickinson, and H. R. Sadeghpour, Phys. Rev. Lett. **85**, 2458 (2000).
[2] S. D. Hogan and F. Merkt, ChemPhysChem **10**, 2931 (2009).
[3] V. Bendkowsky, B. Butscher, J. Nipper, J. P. Shaffer, R. Löw, and T. Pfau, Nature (London) **458**, 1005 (2009).
[4] V. Bendkowsky, B. Butscher, J. Nipper, J. B. Balewski, J. P. Shaffer, R. Löw, T. Pfau, W. Li, J. Stanojevic, T. Pohl, and J. M. Rost, Phys. Rev. Lett. **105**, 163201 (2010).
[5] B. Butscher, J. Nipper, J. B. Balewski, L. Kukota, V. Bendkowsky, R. Löw, and T. Pfau, Nat. Phys. **6**, 970 (2010).
[6] B. Butscher, V. Bendkowsky, J. Nipper, J. B. Balewski, L. Kukota, R. Löw, T. Pfau, W. Li, T. Pohl, and J. M. Rost, J. Phys. B **44**, 184004 (2011).
[7] W. Li, T. Pohl, J. M. Rost, S. T. Rittenhouse, H. R. Sadeghpour, J. Nipper, B. Butscher, J. B. Balewski,

V. Bendkowsky, R. Löw, and T. Pfau, Science **334**, 1110 (2011).
[8] J. Tallant, S. T. Rittenhouse, D. Booth, H. R. Sadeghpour, and J. P. Shaffer, Phys. Rev. Lett. **109**, 173202 (2012).
[9] C. H. Greene, E. L. Hamilton, H. Crowell, C. Vadla, and K. Niemax, Phys. Rev. Lett. **97**, 233002 (2006).
[10] C. Vadla, V. Horvatic, and K. Niemax, Phys. Rev. A **80**, 052506 (2009).
[11] C. Boisseau, I. Simbotin, and R. Côté, Phys. Rev. Lett. **88**, 133004 (2002).
[12] S. M. Farooqi, D. Tong, S. Krishnan, J. Stanojevic, Y. P. Zhang, J. R. Ensher, A. S. Estrin, C. Boisseau, R. Côté, E. E. Eyler, and P. L. Gould, Phys. Rev. Lett. **91**, 183002 (2003).
[13] K. R. Overstreet, A. Schwettmann, J. Tallant, D. Booth, and J. P. Shaffer, Nat. Phys. **5**, 581 (2009).
[14] E. Reinhold and W. Ubachs, Mol. Phys. **103**, 1329 (2005).
[15] A. Kirrander, S. Rittenhouse, M. Ascoli, E. E. Eyler, P. L. Gould, and H. R. Sadeghpour, Phys. Rev. A **87**, 031402 (2013).
[16] A. Omont, J. Phys. France **38**, 1343 (1977).
[17] E. L. Hamilton, C. H. Greene, and H. R. Sadeghpour, J. Phys. B **35**, L199 (2002).
[18] C. Bahrim and U. Thumm, Phys. Rev. A **61**, 022722 (2000).
[19] A. A. Khuskivadze, M. I. Chibisov, and I. I. Fabrikant, Phys. Rev. A **66**, 042709 (2002).
[20] A. Junginger, J. Main, and G. Wunner, Phys. Rev. A **86**, 012713 (2012).
[21] A. Yiannopoulou, G.-H. Jeung, S. J. Park, H. S. Lee, and Y. S. Lee, Phys. Rev. A **59**, 1178 (1999).
[22] For the ground-state potential, $V(R) = -(C_6/R^6)$, $C_6 = 4660$ a.u. (see Ref. [9]). The resulting correction between difference PECs and regular PECs is less than $0.5\,\mathrm{cm}^{-1}$ at $R = 35a_0$.
[23] A.-R. Allouche and M. Aubert-Frécon, J. Chem. Phys. **136**, 114302 (2012).
[24] M. A. Bellos, R. Carollo, J. Banerjee, M. Ascoli, A.-R. Allouche, E. E. Eyler, P. L. Gould, and W. C. Stwalley, Phys. Rev. A **87**, 012508 (2013).
[25] J. Lozeille, A. Fioretti, C. Gabbanini, Y. Huang, H. K. Pechkis, D. Wang, P. L. Gould, E. E. Eyler, W. C. Stwalley, M. Aymar, and O. Dulieu, Eur. Phys. J. D **39**, 261 (2006).
[26] M. Salour, Opt. Commun. **22**, 202 (1977).
[27] E. E. Eyler, A. Yiannopoulou, S. Gangopadhyay, and N. Melikechi, Opt. Lett. **22**, 49 (1997).
[28] Y. Huang, J. Qi, H. K. Pechkis, D. Wang, E. E. Eyler, P. L. Gould, and W. C. Stwalley, J. Phys. B **39**, S857 (2006).
[29] T. Köhler, K. Góral, and P. S. Julienne, Rev. Mod. Phys. **78**, 1311 (2006).
[30] We calculate outer turning points using the $a\,^3\Sigma_u^+$ PEC of C. Strauss, T. Takekoshi, F. Lang, K. Winkler, R. Grimm, J. Hecker Denschlag, and E. Tiemann, Phys. Rev. A **82**, 052514 (2010) and the LEVEL8.0 computer program [see R. J. LeRoy, LEVEL8.0: A Computer Program for Solving the Radial Schrödinger Equation for Bound and Quasibound Levels, University of Waterloo Chemical Physics Research Report CP-663, 2007, http://scienide2.uwaterloo.ca/~rleroy/level/] to solve for the binding energies of levels, and hence their turning points.
[31] S. A. Bhatti, C. L. Cromer, and W. E. Cooke, Phys. Rev. A **24**, 161 (1981).